Dalton Transactions

ARTICLE

Exploring transition metal fluoride chelates – synthesis, properties and prospects towards potential PET probes

Received 00th January 20xx,
Accepted 00th January 20xx

DOI: 10.1039/x0xx00000x

www.rsc.org/

Philip J Blower,[a] William Levason,[b] Sajinder K. Luthra,[c] Graeme McRobbie,[c] Francesco M. Monzittu,*[b] Thomas O. Mules,[b] Gillian Reid,*[b] and M. Nadeem Subhan[b]

The coordination chemistry of the first row transition metal trifluorides with terpy (2,2':6',2''-terpyridine) and Me_3-tacn (1,4,7-trimethyl-1,4,7-triazacyclononane) was explored to identify potential systems for ^{18}F radiolabelling. The complexes $[MF_3(L)]$ (M = Cr, Mn, Fe, Co; L = Me_3-tacn, terpy) were synthesised and fully characterised by UV-vis and IR spectroscopy, microanalysis, and, for the diamagnetic $[CoF_3(L)]$, using ^1H, $^{19}F\{^1H\}$ and ^{59}Co NMR spectroscopy. Single crystal X-ray analyses are reported for $[MF_3(Me_3\text{-tacn})]$ (M = Mn, Co), $[FeF_3(terpy)]$ and $[FeF_3(BnMe_2\text{-tacn})]$. Stability tests on $[MF_3(Me_3\text{-tacn})]$ (M = Cr, Mn, Fe) and $[M'F_3(terpy)]$ (M' = Cr, Fe) were performed and $Cl/^{19}F$ halide exchange reactions on $[CrCl_3(Me_3\text{-tacn})]$ using $[Me_4N]F$ in anhydrous MeCN solution, and $[FeCl_3(Me_3\text{-tacn})]$ using $[Me_4N]F$ in anhydrous MeCN or KF in aqueous MeCN solution were also carried out. Halide exchange reactions proved to be successful in forming $[FeF_3(Me_3\text{-tacn})]$ in aqueous MeCN solution within 30 minutes. Based upon the clean Cl/F exchange and the good stability observed for $[FeF_3(Me_3\text{-tacn})]$ in a range of competitive media, this was identified as a possible candidate for radiolabelling. $^{18}F/^{19}F$ isotopic exchange was achieved by addition of $[^{18}F]F^-$ in the cyclotron target water to a MeCN solution of the benzyl-substituted analogue, $[FeF_3(BnMe_2\text{-tacn})]$, at a range of concentrations down to 24 nM with heating to 80 °C for 10 mins.; the resulting $[Fe^{18}F^{19}F_2(BnMe_2\text{-tacn})]$ shows radiochemical purity (RCP) ≥ 90% after 2 h in a range of formulations, including 10% EtOH/phosphate buffered saline (PBS) and 10% EtOH/human serum albumin (HSA). This is the first reported complex with a transition metal directly bonded to $[^{18}F]F^-$.

Introduction

C-^{18}F based radiotracers are extensively used in positron emission tomography (PET) for imaging purposes in oncology, cardiology and neurology.[1] Thousands of PET scans are performed daily on cancer patients worldwide, providing important diagnostic and clinical information. Peptides that target receptors overexpressed on the surface of the diseased cells are becoming increasingly important in diagnostic PET imaging agents.[2] However, the reaction conditions for the formation of the C-^{18}F bond are often incompatible with biomolecules (e.g. peptides).[3] Organic solvents that degrade the peptide, high temperatures and competing sites for the ^{18}F-labelling reaction present in the biomolecule, are the major problems encountered. As a result, often the $[^{18}F]F^-$ is first incorporated into an organic molecule (prosthetic group) and then conjugated to a peptide, resulting in an increase of the total reaction time and the number of steps of the process.[3] The need to improve these aspects has led to the investigation of alternative non-C-^{18}F moieties. To date, several main group elements attached to $[^{18}F]F^-$ have been studied, including boron-,[4] aluminium-,[5,6] gallium-,[7,8] sulfur-,[9] and silicon-fluoride[10] systems. These are discussed in recent reviews.[11] The two Group 13 metals are often coordinated to macrocyclic ligands (triazacyclononane derivatives) which confer thermodynamic and kinetic stability to the chelates and, in the case of the systems with 1,4-dimethyl-7-benzyl-1,4,7-triazacyclononane ($BnMe_2$-tacn), the benzyl group provides a site for further functionalisation and bioconjugation.[6,7] In this approach to PET radiotracers based on metal coordination complexes, the stability of the complex will be strongly dependant on the properties of the metal centre. The M-F bond dissociation energy has an important role since it should be stronger compared to M-Cl, hence allowing fluorination through halide exchange reactions and, ultimately, it should be resistant in physiological conditions. Other aspects related to the metal to be considered are its size (dictating the coordination number), its redox chemistry and oxophilicity (water or anions such as phosphate should not disrupt the coordination around the metal), its Lewis acidity and its lability, allowing sufficiently rapid substitution of fluoride into the

[a] School of Biomedical Engineering and Imaging Sciences, King's College London, St Thomas' Hospital, London SE1 7EH, UK
[b] Chemistry, University of Southampton, Highfield, Southampton SO17 1BJ, UK. *E-mail: G.Reid@soton.ac.uk; F.Monzittu@soton.ac.uk
[c] Pollards Wood, Nightingales Lane, Chalfont St Giles, Bucks, HP8 4SP, UK.

† Electronic supplementary information (ESI) available: X-ray crystallographic parameters are given in table S1. The ESI also contains UV-vis, IR and NMR spectra of the complexes, UV-vis spectra of the stability tests for $[MF_3(Me_3\text{-tacn})]$ (M = Mn, Fe) and $[MF_3(terpy)]$ (M = Cr, Fe), figures showing the π-stacking and H-bonding in $[FeF_3(terpy)]$ and H-bonding in $[CoF_3(Me_3\text{-tacn})]$ and $[FeF_3(BnMe_2\text{-tacn})]$, and radio and UV-traces for the radiofluorination experiments. See DOI: 10.1039/x0xx00000x

coordination sphere (when the ^{18}F half-life of 110 mins. is considered).

We previously developed the chemistry of the Group 13 metal fluorides (Al, Ga) towards neutral nitrogen ligands and reported that radioactive ^{18}F can be introduced into $[MCl_3(BnMe_2\text{-tacn})]$ (M = Al, Ga) through Cl/^{18}F halide exchange reactions and that $[GaF_3(BnMe_2\text{-tacn})]$ can also be ^{18}F-radiolabelled through $^{18}F/^{19}F$ isotopic exchange using a very small amount of material (27 nmol); both methods were successful in mild conditions, i.e. aqueous solution, room temperature or 80°C.[6,7,12] We also investigated the transition metal fluorides using Sc(III), Y(III), La(III) and Lu(III).[13] Among these d- and f-block metal systems, only the $[ScF_3(RMe_2\text{-tacn})]$ (R = Me, Bn) were successfully synthesised through Cl/F halide exchange reactions. $[ScF_3(BnMe_2\text{-tacn})]$ was identified as a promising system for future ^{18}F-radiolabelling, although, in contrast to the Group 13 systems, it could only be obtained from the trichloride analogue under anhydrous conditions using $[NMe_4]F$ or Me_3SnF as the fluoride source. However, the trifluoride complex is very stable in water.[13]

In this work, we present an evaluation of the 3*d* transition metal (Cr^{3+}, Mn^{3+}, Fe^{3+} and Co^{3+}) trifluoride complexes for possible PET applications. The distorted octahedral MF_3 complexes bearing tridentate Me_3-tacn and terpy ligands, are described and their stabilities in water probed by UV-vis spectroscopy. Their properties are discussed in order to identify the best prospects for fluorination for future possible applications in PET. Finally, we demonstrate successful $^{18}F/^{19}F$ isotopic exchange using $[FeF_3(BnMe_2\text{-tacn})]$, and confirm its stability in ethanolic phosphate buffered saline (PBS) or human serum albumin (HSA) over at least 2 h.

In setting out the scope for this study, Ti^{3+} and V^{3+} were not considered as the former is very readily oxidised, while the latter is also likely to form V(IV) in aqueous solution. Previous work has shown that $[VOF_2(Me_3\text{-tacn})]$ is readily obtained by adding a few drops of water to a methanol solution of $[VF_3(Me_3\text{-tacn})]$ in air.[14] Nickel was also excluded as no trifluoride complexes are known and Ni(III) is reduced in water.[15] The ligand substitution kinetics for the majority of second and third row transition metal complexes are expected to be too slow to allow sufficiently fast halide substitution, given the short ½-life of the ^{18}F radionuclide.

The electronic configurations of the 3*d* metal ions influence their reactivity and the kinetic robustness of the complexes formed. Neutral trifluoride complexes of these metals are scarce or unknown, in contrast to the heavier halides. Octahedral d^3 Cr(III) mono-, di- and tri-fluoride complexes with N-donor ligands have been reported.[16] In particular, complexes of ammonia and amines have been studied extensively for their absorption and emission properties, contributing to the development of inorganic electronic spectroscopy.[17] The neutral species $[CrF_3(bipy)(OH_2)]$,[18] *fac*-$[CrF_3(Me_3\text{-tacn})]$[19,20] and *mer*-$[CrF_3(terpy)]$[20] have also been reported and structurally characterised. Complexes with tetradentate N-donor ligands can also be found in the literature.[21] Neutral complexes of Mn(III) trifluoride with N-donor ligands are known, with the structures of $[MnF_3(bipy)(OH_2)]$,[22] $[MnF_3(phen)(OH_2)]$,[23] $[MnF_3(terpy)]$[24] and $[\{MnF_2(Me_3\text{-tacn})\}_2(\mu\text{-}F)][PF_6]$[25] reported. The d^4 configuration associated with Mn(III) causes a Jahn-Teller distortion, a feature exploited in the synthesis of molecular magnets.[26] Iron(III) trifluoride complexes reported in the literature include *mer*-$[FeF_3(NH_3)_3]$[27] and *fac*-$[FeF_3(Me_3\text{-tacn})]$.[19] While octahedral Co(III) complexes with amine ligands have long been known,[28] no crystal structures of neutral Co(III) trifluoride complexes with N-donor or O-donor ligands have been reported. *Mer*-$[CoF_3(NH_3)_3]$ has been characterised spectroscopically.[29] The coordination chemistry of transition metal fluoride complexes has been reviewed recently,[30] including their complexes with neutral ligands.[15]

Experimental

Synthetic procedures and characterisation details are presented in the ESI.

$^{18}F/^{19}F$ Isotopic Exchange Radiolabelling Procedure: In a typical experiment, $[FeF_3(BnMe_2\text{-tacn})]\cdot 3.5H_2O$ (1 mg, 2.36 µmol, 0.1 mg, 236 nmol or 0.01 mg, 24 nmol) was dissolved in MeCN (n = 8) (0.75 mL). To this solution was added 0.25 mL of an aqueous solution containing $[^{18}F]F^-$ (40-180 MBq) and the vial was heated to 80 °C for 10 mins. The crude reaction solution was diluted with water (20 mL) so that approximately 10% of the solvent composition was organic. A small sample (~ 100 uL) of the diluted crude reaction solution was removed for analysis by analytical HPLC, which confirmed the percentage incorporation of $[^{18}F]F^-$ into the metal complex (based upon integration of the radio peaks). Approximately 6% $[^{18}F]F^-$ incorporation was observed when the radiolabelling experiment was performed using 1 mg of the iron complex in $MeCN/H_2O$ (75:25) at room temperature. The product was purified by either a SPE process or by HPLC.

SPE Purification Protocol: The diluted reaction mixture was trapped on a HLB cartridge, washed with water (5 mL x 3) to remove the residual $[^{18}F]F^-$ and MeCN and then the product was eluted from the cartridge with ethanol (1 mL) into either (i) water to result in a formulated product in 80:20 water:EtOH; (ii) PBS to result in a formulated product in 90:10 PBS:EtOH or (iii) HSA to result in a formulated product in 90:10 HSA:EtOH. The formulated product was analysed by HPLC at t = 0 and various time intervals up to 120 mins.

Experiments were analysed on an Agilent 1290 HPLC system with an Agilent 1260 DAD UV detector (G4212B). Dionex Chromeleon 6.8 Chromatography data recording software was used to integrate the radiochemical peak areas.

Analytical HPLC method: Column: Phenomenex Luna 5 um C18(2) 250 x 4.6 mm. Mobile phase A = water, B = MeCN. Flow rate 1 mL min^{-1}. Gradient 0-15 min (10-90 % B), 15-20 min (90 % B), 20-21 min (90-10 % B), 21-26.5 min (10 % B).

HPLC purification: Column: Waters XBridge Prep Shield RP18, 5 um, 10 x 100 mm (p/n 186003258); Dionex Ultimate 3000 pump; Knauer Smartline 2500 UV detector. Mobile phase A = water; B = MeCN). Flow rate 3 mL min^{-1}. Gradient 0-10 min (0-10% B), 10-15 min (10-90% B), 15-20 min (90% B), 20-25 min (90-2% B).

Results and discussion

The syntheses of the complexes [MF_3(L)] (M = Cr, Mn, Fe, Co; L = terpy, Me_3-tacn) were carried out in alcoholic (n-BuOH or EtOH) or dmf solutions at room temperature or under reflux (Scheme 1) and the products were characterised by IR spectroscopy, microanalysis and UV-vis spectroscopy (diffuse reflectance and solution).

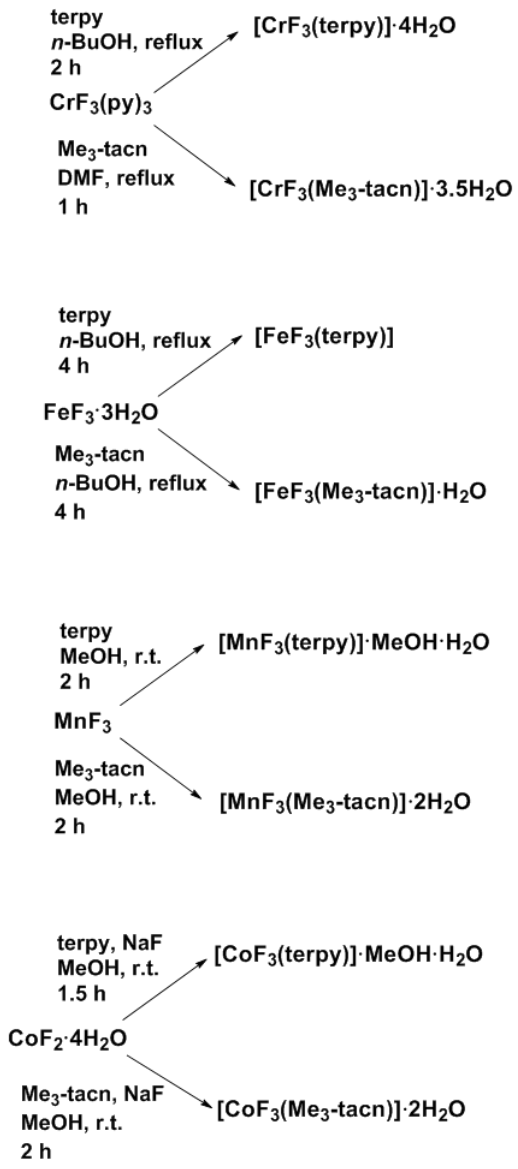

Scheme 1. Reaction conditions for the preparation of the complexes.

The trifluoro complexes have a strong tendency to form H-bonding interactions between the fluorides and water molecules in the lattice;[8] this has often led to discrepancy in the number of water molecules co-crystallised in the lattice compared to the literature[19,20,24] and in some cases in this work leading to differences in the number of associated water molecules between the bulk materials and the crystal structures (for example [MF_3(Me_3-tacn)], M = Mn, Co, have two water molecules in the bulk, but four in the crystal structure). This might be due to differences in the crystallisation methods employed and the length of time the bulk materials were dried *in vacuo*. The products are air stable and can be stored outside the glovebox for several weeks. The stability of the complexes was challenged in aqueous solution by the presence of up to 10-fold excess of competitive ions (NaCl, NaF, Na_2CO_3, Na_3PO_4, NaOAc), increased temperature and changes in pH at two different time points (t = 0 and t = 4 h). UV-vis spectroscopy was used to monitor the solutions, changes in the position of the relevant *d-d* transitions and or appearance/disappearance of bands were taken as an indication of the instability of the complex during the experiments.

Chromium: *Mer*-[CrF_3(terpy)]·$4H_2O$ and *fac*-[CrF_3(Me_3-tacn)]·$3.5H_2O$ were obtained as purple solids in good yields by reaction of [$CrF_3(py)_3$] with the ligands in n-BuOH or dmf, respectively, following literature methods.[20] The IR spectra of the solids confirm the presence of water and show two ν(Cr-F) bands for CrF_3(Me_3-tacn)]·$3.5H_2O$, as expected for a *fac* octahedral configuration in C_{3v} symmetry, whereas one very broad band is seen for [CrF_3(terpy)]·$4H_2O$ (three bands are expected in a *mer* C_{2v} symmetry, but not resolved). The diffuse reflectance spectra of the complexes are shown in Figure S8 and S12, and resemble those reported previously.[20]

Manganese: The reaction of MnF_3 with Me_3-tacn or terpy in anhydrous MeOH at room temperature produces the species [MnF_3(Me_3-tacn)]·$3H_2O$ and [MnF_3(terpy)]·MeOH·$3H_2O$, respectively. The presence of MeOH in [MnF_3(terpy)]·MeOH·$3H_2O$ was confirmed by ^{1}H NMR spectroscopy (CD_3CN, δ = 3.28 (CH_3OH), 2.15 (CH_3OH)). The molecular composition of [MnF_3(Me_3-tacn)] was confirmed by a single crystal X-ray structure analysis (Fig. 1).

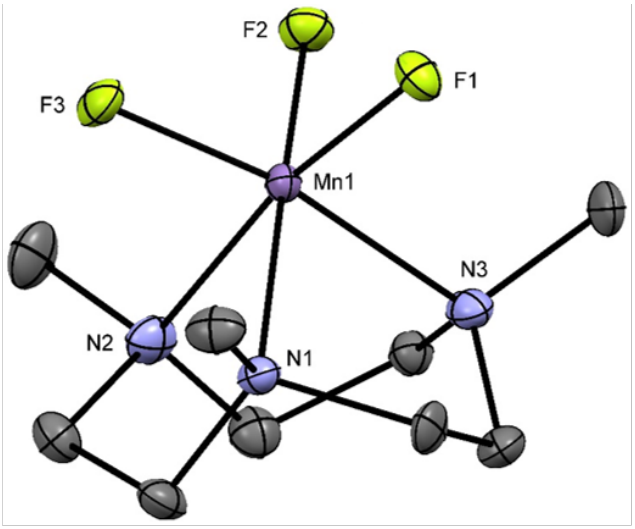

Figure 1. Crystal structure of *fac*-[MnF_3(Me_3-tacn)]·$4H_2O$ with ellipsoids drawn at the 50 % probability level. H atoms and water molecules are omitted for clarity. Selected bond lengths (Å) and angles (°): Mn1–F1 = 2.017(2), Mn1–F2 = 1.852(2), Mn1–F3 = 1.848(2), Mn1–N1 = 2.080(3), Mn1–N2 = 2.267(3), Mn1–N3 = 2.096(3), F1–Mn1–N1 = 91.29(10), F3–Mn1–N3 = 170.31(11), F2–Mn1–N1 = 172.65(10), F1–Mn1–F3 = 94.88(9), F1–Mn1–F2 = 94.43(9), N1–Mn1–N2 = 80.92(11), N1-Mn1-N3 = 83.43(11).

The structure shows a distorted octahedral environment with the fluorides *facially* coordinated to the metal. The Mn-F3 and Mn-N3 bond lengths are elongated by ~0.17 Å and ~0.18 Å compared to the other Mn-F and Mn-N distances, respectively.

This significant difference in the bond lengths is consistent with a Jahn-Teller distortion in the high spin d^4 configuration.[16] As confirmation of this, the complex has a magnetic moment of 4.94 BM.[31] The tetragonal elongation in the related complex $[\{MnF_2(Me_3\text{-tacn})\}_2(\mu\text{-F})][PF_6]$[25] is observed along the axis on which Mn-$F_{bridging}$ and Mn-N *trans* to it lie. These bond lengths are ~0.18 and ~0.23 Å longer than the other Mn-N and Mn-F bonds, respectively.[25] The Mn-$F_{terminal}$ distance in $[\{MnF_2(Me_3\text{-tacn})\}_2(\mu\text{-F})][PF_6]$ is ~0.03 Å shorter than Mn1-F1 and Mn1-F2 in $[MnF_3(Me_3\text{-tacn})]\cdot 2H_2O$. Extensive H-bonding involving the water molecules and the fluorides is also present (Fig. 2). The same H-bonding pattern was observed in $[GaF_3(Me_3\text{-tacn})]\cdot 4H_2O$.[8]

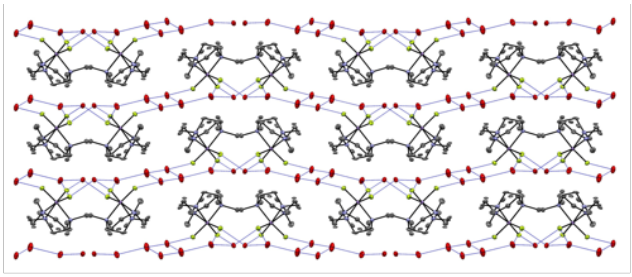

Figure 2. H-bonding interaction present in $[MnF_3(Me_3\text{-tacn})]\cdot 4H_2O$.

The diffuse reflectance UV-vis spectrum of $[MnF_3(Me_3\text{-tacn})]\cdot 4H_2O$ (Fig. S19) shows intense bands in the UV region due to ligand to metal charge transfer transitions (σN→Mn) and a single *d-d* transition at ~520 nm, generically assigned to $^5E_g \rightarrow {}^5T_{2g}$. Although in an octahedral d^4 high spin configuration only one spin-allowed transition is predicted ($^5E_g \rightarrow {}^5T_{2g}$), Jahn-Teller distortions can often lower the symmetry, resulting in splitting of the single transition. However, in this case splitting is not resolved. These data resemble those of the dimer $[\{MnF_2(Me_3\text{-tacn})\}_2(\mu\text{-F})][PF_6]$.[25]

Splitting is more resolved in $[MnF_3(terpy)]\cdot MeOH\cdot 3H_2O$ (Fig. S15) and the three bands shown in the spectra are tentatively assigned to $^5B_{1g} \rightarrow {}^5A_{1g}$, $^5B_{1g} \rightarrow {}^5B_{2g}$, $^5B_{1g} \rightarrow {}^5E_g$. The metal centre symmetry is C_{2v} and it is possible that both this and the Jahn-Teller effect results in greater splitting of the bands compared to $[MnF_3(Me_3\text{-tacn})]\cdot 2H_2O$. Strong absorptions at high energy, due to the LMCT transitions, σN→Mn, and π-π* transitions within the aromatic rings, are also present.

Iron: $[FeF_3(Me_3\text{-tacn})]\cdot H_2O$ was obtained as a pale yellow solid (in contrast to the green colour reported previously in the literature[19]) after reaction of $FeF_3\cdot 3H_2O$ with Me_3-tacn in refluxing n-BuOH. Its IR spectrum shows the expected two ν(Fe-F) bands at 512 and 529 cm^{-1}. $[FeF_3(terpy)]\cdot 2H_2O$, made using the same method, was obtained as a light purple powder and characterised similarly. The diffuse reflectance UV-vis spectra of the complexes are shown in Figs. S26 and S30. The electronic transitions in a d^5 high spin system with a ground state $^6A_{1g}$ are all spin-forbidden and weak bands in the visible region are therefore seen.

Crystals suitable for single crystal X-ray analysis of $[FeF_3(terpy)]\cdot 3H_2O$ were obtained by slow evaporation of a concentrated solution of the complex in water (Fig. 3).

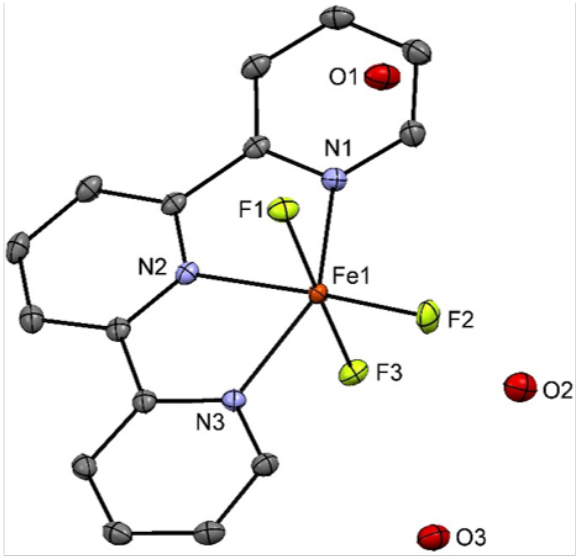

Figure 3. Crystal structure of *mer*-$[FeF_3(terpy)]\cdot 3H_2O$ with ellipsoids drawn at the 50 % probability level. H atoms are omitted for clarity. Selected bond lengths (Å) and angles (°): Fe1–F1 = 1.8774(8), Fe1–F2 = 1.8563(8), Fe1–F3 = 1.9062(8), Fe1–N1 = 2.1564(12), Fe1–N2 = 2.1144(12), Fe1–N3 = 2.1410(11), F1–Fe1–N1 = 88.03(4), F3–Fe1–N3 = 89.78(4), F2–Fe1–N1 = 110.00(4), F1–Fe1–F3 = 176.33(4), F1–Fe1–F2 = 91.20(4), N1–Fe1–N2 = 74.69(4), N1-Fe1-N3 = 149.17(4), F2-Fe1-N2 = 174.92(4).

The structure shows a *meridional* configuration around the metal. The Fe-F bond lengths are slightly longer than those in $[FeF_3(Me_3\text{-tacn})]\cdot H_2O$[19] (1.878-1.907 Å *vs.* 1.850-1.866 Å) whereas the opposite trend is seen in the Fe-N bonds with the terpy complex having the shortest Fe-N distance (2.142-2.156 *vs.* 2.223-2.228). The rigidity of the terpy ligand forces some of the angles to deviate from the 180/90° expected for an

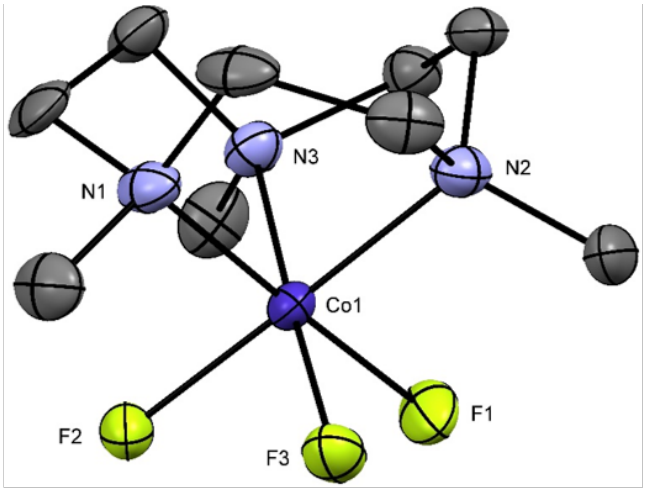

Figure 4. Crystal structure of *fac*-$[CoF_3(Me_3\text{-tacn})]\cdot 4H_2O$ with ellipsoids drawn at the 50 % probability level. H atoms and water molecules are omitted for clarity. Selected bond lengths (Å) and angles (°): Co1–F1 = 1.857(3), Co1–F2 = 1.871(2), Co1–F3 = 1.871(3), Co1–N1 = 1.960(4), Co1–N2 = 1.960(4), Co1–N3 = 1.958(4), F1–Co1–N1 = 178.30(14), F3–Co1–N3 = 178.13(14), F2–Co1–N1 = 91.39(14), F1–Co1–F3 = 88.29(13), F1–Co1–F2 = 89.92(12), N1–Co1–N2 = 87.62(16), N1-Co1-N3 = 87.95(15).

octahedron. Extensive H-bonding and π-stacking interactions are also present in the lattice (Fig. S1).

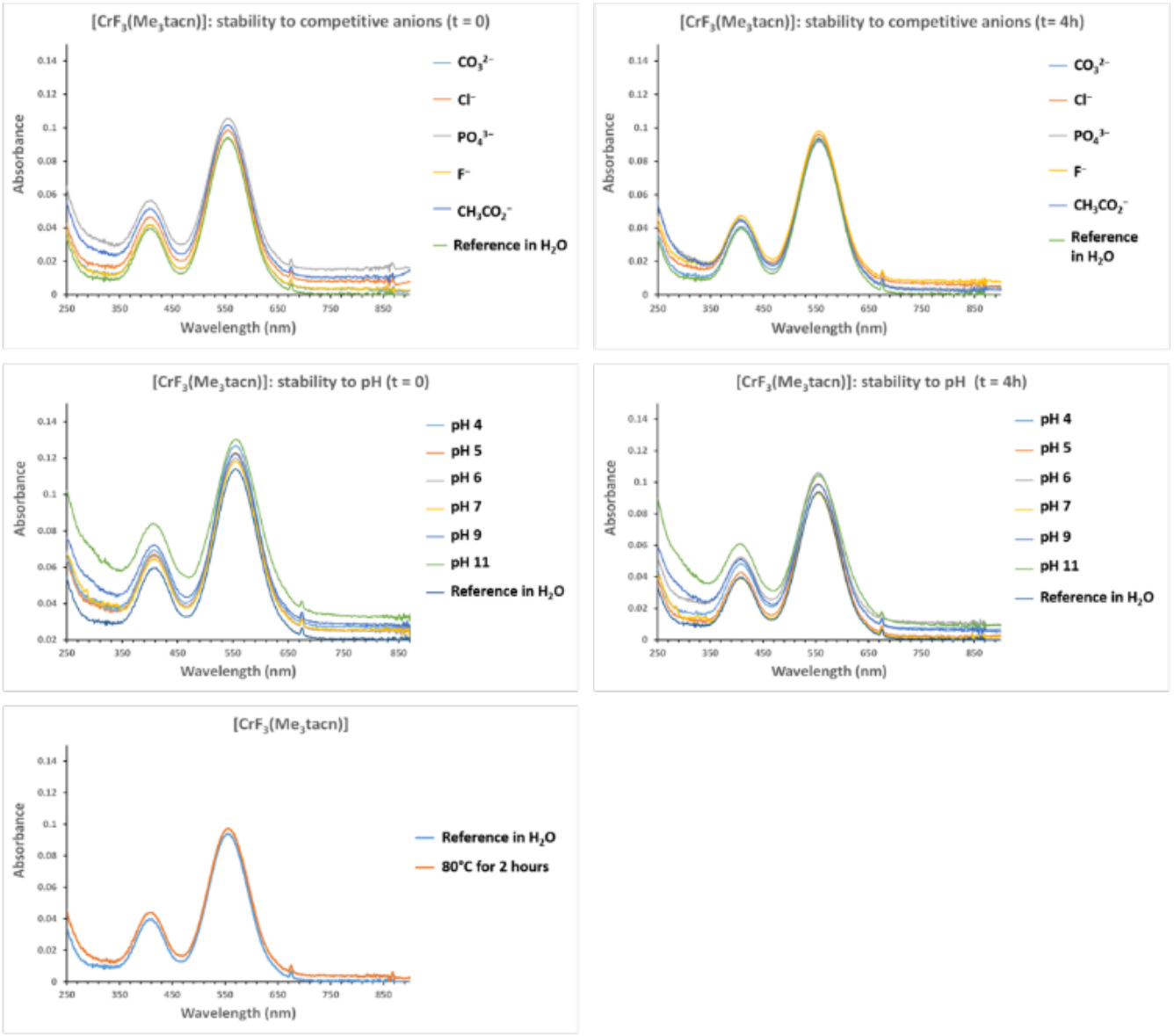

Figure 5. Stability test of $[CrF_3(Me_3\text{-tacn})]\cdot 3.5H_2O$. First row from the top: UV-vis spectra of the complex in the presence of a 10-fold excess anions at (left) t = 0 and (right) t = 4 hours; middle row: UV-vis spectra of the complex at different pH conditions at (left) t = 0 and (right) t = 4 hours; bottom row: UV-vis spectra of the complex after two hours at 80 °C.

Cobalt: $[CoF_3(Me_3\text{-tacn})]\cdot 2H_2O$ and $[CoF_3(terpy)]\cdot MeOH\cdot H_2O$ were prepared by oxidising $CoF_2\cdot 4H_2O$ to Co(III) in air in the presence of NaF and the appropriate ligand. The reactions were carried out in MeOH at room temperature. The complexes were characterised by UV-vis and IR spectroscopy and by ^{1}H, $^{19}F\{^{1}H\}$ and ^{59}Co NMR spectroscopy, given the diamagnetic d^6 low spin electronic configuration of the complexes. The $^{19}F\{^{1}H\}$ NMR spectra of the complexes in CD_3OD show broad resonances, with no resolved $^{1}J_{F\text{-}Co}$ coupling, at −149 ($[CoF_3(Me_3\text{-tacn})]\cdot 2H_2O$) and −116 ppm ($[CoF_3(terpy)]\cdot MeOH\cdot H_2O$). The ^{59}Co (I = 7/2, Q = $0.42\cdot 10^{-28}$ m^2)[32] NMR spectra show very broad peaks at ~ 9000 and 8600 ppm respectively, which are in the range of other octahedral Co(III) complexes, such as $[Co(NH_3)_6]^{3+}$ and $[Co(en)_3]^{3+}$.[33] However, when the spectrum of $[CoF_3(Me_3\text{-tacn})]\cdot 2H_2O$ is recorded in D_2O solution, the $^{19}F\{^{1}H\}$ NMR resonance associated with the complex is lost and only F^- is present (118.9 ppm). Crystals of $[CoF_3(Me_3\text{-tacn})]\cdot 2H_2O$ (Figure 4) were grown from a concentrated solution in water.

The UV-vis diffuse reflectance spectra of the complexes are shown in Figs. S34, S40. The two spin-allowed transitions predicted for a low spin d^6 system are present in the spectrum of *fac*-$[CoF_3(Me_3\text{-tacn})]$ (Fig. S40) at ~570 and ~375 nm and are assigned to $^{1}A_{1g}\rightarrow{}^{1}T_{1g}$ and $^{1}A_{1g}\rightarrow{}^{1}T_{2g}$, respectively. The *mer*-$[CoF_3(terpy)]\cdot MeOH\cdot H_2O$ has C_{2v} symmetry and splitting is greater than in the Me_3-tacn complex (C_{3v}). The $^{1}T_{1g}$ level split into three components and the transitions observed are tentatively assigned to $^{1}A_{1g}\rightarrow{}^{1}B_{1g}$, $^{1}A_{1g}\rightarrow{}^{1}B_{2g}$ and $^{1}A_{1g}\rightarrow{}^{1}B_{3g}$ (Fig. S34, from low to high energy).[17,34] In this case, the third (higher energy) spin-allowed transition $^{1}A_{1g}\rightarrow{}^{1}T_{2g}$ is masked by the ligand to metal charge transfer and/or π-π^* bands involving the terpy ligand. Crystals of $[CoF_3(Me_3\text{-tacn})]\cdot 4H_2O$ suitable for single crystal X-ray analysis were obtained by slow evaporation of a concentrated solution of the complex in water (Figure 4).

The complex is isostructural to $[MnF_3(Me_3\text{-tacn})]\cdot 4H_2O$ and shows the same H-bonding pattern in the lattice (Fig. S2).

Stability tests: The stability of a 10^{-3} M solution of the complexes $[MF_3(Me_3\text{-tacn})]$ (M = Cr, Mn, Fe) and $[M'F_3(terpy)]$ (M = Cr, Fe) was challenged in the presence of up to a 10-fold excess of competitive ions (F^-, Cl^- CO_3^{2-}, PO_4^{3-}, AcO^-, added as sodium salts), pH variations (4-11), temperature (80°C for 2 h) and time. The spectra acquired were compared with the spectra of the relevant reference complex. Given the limited stability of $[CoF_3(Me_3\text{-tacn})]\cdot 2H_2O$ in water, stability tests were not carried out on this complex.

$[CrF_3(Me_3\text{-tacn})]\cdot 3.5H_2O$ appears to be stable under all conditions tested (Fig. 5), whereas $[CrF_3(terpy)]\cdot 4H_2O$ is not stable in the presence of PO_4^{3-} after 4 h (the 558 nm band shifts to lower energy by ~10 nm). Both complexes are unaffected by heating at 80 °C for 2 h and after standing for an extended period (one week) in aqueous solution (Fig. S11, 5).

The stability of the Mn(III) complex is inferior to that of the Cr(III) analogue, as expected for a d^4 system. $[MnF_3(Me_3\text{-tacn})]\cdot 2H_2O$ (Fig. S23) is stable to the presence of excess chloride and fluoride, but is unstable to phosphate, acetate and carbonate even at t = 0, with no significant further change observed after 4 h. Moreover, pH > 4 also results in the decomposition of the complex, as also observed upon heating and prolonged exposure in aqueous solution. Decomposition of the sample was clearly observable as a black solid formed, most likely MnO_2 or MnO(OH). Considering the already problematic stability of $[MnF_3(Me_3\text{-tacn})]\cdot 2H_2O$, the stability tests on $[MnF_3(terpy)]\cdot MeOH\cdot 3H_2O$ were not pursued.

The results of the stability tests on $[FeF_3(Me_3\text{-tacn})]\cdot H_2O$ are shown in Figure S33. The complex is stable to the presence of all the anions studied at t = 0. However, the spectra acquired after 4 h show that the presence of carbonate anions causes decomposition of the complex. Similar behaviour was observed in the pH 7 experiment (stable at t = 0 and unstable at t = 4 h), whereas the complex is unstable at pH 11 from t = 0. The complex is stable after 2 h at 80 °C in water and is unchanged after one week in aqueous solution. The stability tests on $[FeF_3(terpy)]\cdot 2H_2O$ in the same conditions (Fig. S29) showed that the positions of the peaks were unchanged, however a change in their intensity and in the colour of the solution of the complex in water from red to pink was observed.

Halide exchange reactions on $[MCl_3(Me_3\text{-tacn})]$ (M = Cr, Fe): Since radioactive $[^{18}F]F^-$ can be incorporated into $[AlCl_3(BnMe_2\text{-tacn})]$, $[GaCl_3(BnMe_2\text{-tacn})]$ and $[GaCl(Bn(CH_2COO)_2\text{-tacn})]$ through Cl^-/F^- exchange reactions,[6,8] this possibility was explored for $[MCl_3(Me_3\text{-tacn})]$ (M = Cr, Fe) through preliminary experiments using non-radioactive $[NMe_4]^{19}F$ or $K^{19}F$ as test reactions on a preparative scale. Given the instability of $[MnF_3(Me_3\text{-tacn})]$ in the majority of the conditions tested and the limited stability of $[CoF_3(Me_3\text{-tacn})]\cdot 2H_2O$ in water, fluorination reactions to form these complexes were not pursued.

The Cl/F substitution on $[CrCl_3(Me_3\text{-tacn})]$ was incomplete after 24 h under reflux in MeCN in the presence of 4 mol. equiv. of $[NMe_4]F$. The crude solid obtained was analysed by IR spectroscopy and compared with the IR spectra of $[CrCl_3(Me_3\text{-tacn})]$ and $[CrF_3(Me_3\text{-tacn})]$ (Fig. S3), showing that the CrF_3-complex is formed during the reaction (ν Cr-F 539, 507 cm^{-1}) but it appears that some $CrCl_3$-complex and/or mixed chloride/fluoride species are still present (ν Cr-Cl 343, 333 cm^{-1}). This is not surprising given the slow substitution kinetics in the d^3 systems. However, much more promisingly, $[FeCl_3(Me_3\text{-tacn})]$ was successfully fluorinated in the presence of either 4 mol. equiv. of $[NMe_4]F$ in anhydrous MeCN under reflux for 4 h or using 4 mol. equiv. of KF in aqueous MeCN at room temperature within 30 mins. $[FeF_3(Me_3\text{-tacn})]$ was isolated after work-up and characterised by IR spectroscopy. Comparison of the IR spectra of the parent $[FeCl_3(Me_3\text{-tacn})]$ and $[FeF_3(Me_3\text{-tacn})]$ with the product obtained from the halide exchange reaction is shown in Fig. 6.

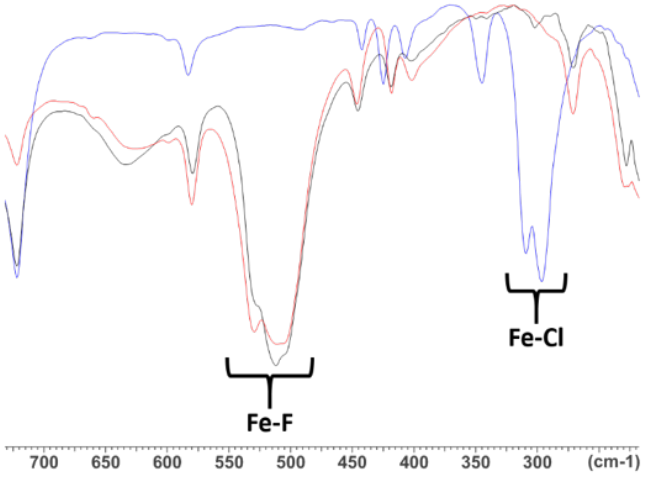

Figure 6. Comparison of the IR spectra of $[FeCl_3(Me_3\text{-tacn})]$ (blue), $[FeF_3(Me_3\text{-tacn})]$ (black) and $[FeF_3(Me_3\text{-tacn})]$ from the halide exchange reaction (red).

It can be seen that the IR spectrum of $[FeF_3(Me_3\text{-tacn})]$ (Fig. 6, red line) obtained by the halide exchange reaction in aqueous MeCN shows the disappearance of the Fe-Cl stretches (~300 and ~310 cm^{-1}, blue line) and the peaks at ~510 and ~525 cm^{-1} match the Fe-F stretches in the spectrum of the reference compound, $[FeF_3(Me_3\text{-tacn})]$ (black line), obtained directly from the reaction of $FeF_3\cdot 3H_2O$ and Me_3-tacn.

These studies suggest that the $[FeF_3(R_3\text{-tacn})]$ system may be worth further investigation as a possible platform for PET applications. In order to test this, the Bn-substituted analogue, $[FeF_3(BnMe_2\text{-tacn})]$ was prepared; the presence of the Bn group aids identification of the final radio-product via UV-vis spectroscopy. The crystal structure (Figure 7) confirms the formulation $[FeF_3(BnMe_2\text{-tacn})]\cdot 2H_2O$, with two co-crystallised water molecules in the lattice. Two crystallographically independent molecules are present in the asymmetric unit, although the bond distances are not significantly different.

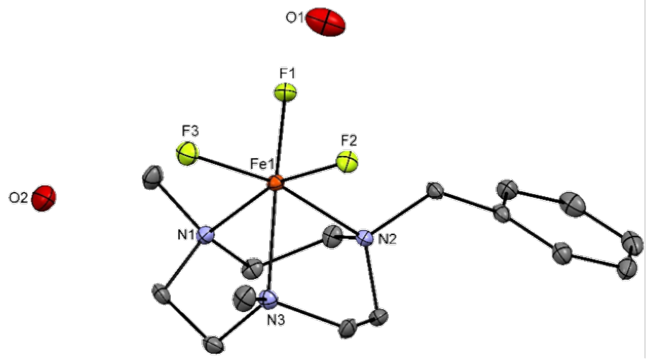

Figure 7. Crystal structure of $[FeF_3(BnMe_2\text{-tacn})]\cdot 2H_2O$ showing the atom numbering scheme and with ellipsoids drawn at the 50% probability level. H atoms are omitted for clarity. Selected bond lengths (Å) and angles (°): Fe1-F1 = 1.8878(19), Fe1-F2 = 1.8673(17), Fe1-F3 = 1.8778(19), Fe1-N1 = 2.206(2), Fe1-N2 = 2.237(3), Fe1-N3 = 2.197(3), F1-Fe1-F2 = 99.00(8), F1-Fe1-F3 = 95.91(8), F2-Fe1-F3 = 99.13(8), F1-Fe1-N3 = 167.58(9), F1-Fe1-N2 = 90.30(9), F1-Fe1-N1 = 91.36(9), F3-Fe1-N2 = 167.08(9), F2-Fe1-N1 = 165.67(8), N1-Fe1-N2 = 78.96(9), N1-Fe1-N3 = 79.32(9), N2-Fe1-N3 = 79.92(10).

Radiofluorination

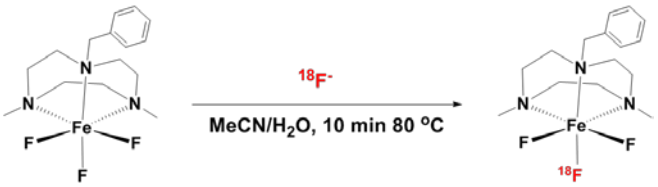

Scheme 2. ^{18}F radiolabelling conditions.

^{18}F-radiofluorination of $[FeF_3(BnMe_2\text{-tacn})]$ was achieved through $^{18}F/^{19}F$ isotopic exchange reactions in unbuffered 75:25 MeCN:H_2O and heating the mixture to 80°C for 10 mins. The water used in the reaction is the target water containing $[^{18}F]F^-$ directly received from the cyclotron, without further purification. The reaction produces $[Fe^{18}F^{19}F_2(BnMe_2\text{-tacn})]$ in a ~40% radiochemical yield (RCY) when starting with 1 and 0.1 mg (2360 and 236 nmol respectively) of $[Fe^{19}F_3(BnMe_2\text{-tacn})]$, along with unreacted $[^{18}F]F^-$.

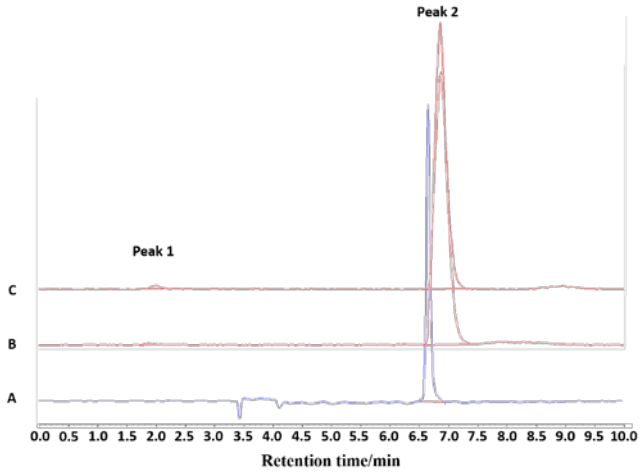

Figure 8. **A**: Analytical UV-HPLC chromatogram of the reference standard compound $[Fe^{19}F_3(BnMe_2\text{-tacn})]$ (Rt = 6.67 min); **B**: analytical radio-HPLC chromatogram of the purified product eluted from a HLB cartridge and formulated in 20:80 EtOH:water at t = 0. Peak 2: Rt = 6.88 min >99% ($[Fe^{18}F^{19}F_2(BnMe_2\text{-tacn})]$); **C**: analytical radio-HPLC chromatogram of the purified product eluted from a HLB cartridge and formulated in 20:80 EtOH:water at t = 120 min. Peak 1: Rt = 1.99 min 1% ($[^{18}F]F^-$). Peak 2: Rt = 6.85 min 99% ($[Fe^{18}F^{19}F_2(BnMe_2\text{-tacn})]$).

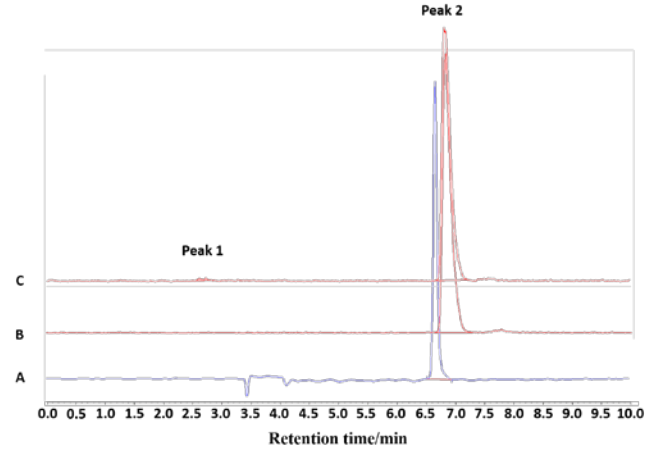

Figure 9. **A**: Analytical UV-HPLC chromatogram of the reference standard compound $[Fe^{19}F_3(BnMe_2\text{-tacn})]$ (Rt = 6.67 min); **B**: analytical radio-HPLC chromatogram of the purified product eluted from a HLB cartridge and formulated in 10:90 EtOH:PBS at t = 0. Peak 2: Rt = 6.88 min >99% ($[Fe^{18}F^{19}F_2(BnMe_2\text{-tacn})]$); **C**: analytical radio-HPLC chromatogram of the purified product eluted from a HLB cartridge and formulated in 10:90 EtOH:PBS at t = 120 min. Peak 1: Rt = 2.73 min 1% ($[^{18}F]F^-$). Peak 2: Rt = 6.82 min 99% ($[Fe^{18}F^{19}F_2(BnMe_2\text{-tacn})]$).

The identity of the radio-product was confirmed by comparison with the UV trace of the inactive reference standard. $[Fe^{19}F_3(BnMe_2\text{-tacn})]$. $[^{18}F]F^-$ incorporation also occurs within 10 mins. at room temperature, although (unsurprisingly) this leads to a considerably lower RCY (6±1%) (Table 1 and Fig S52 in ESI). Radiofluorination was also achieved using 0.01 mg (24 nmol) of precursor (80°C/10 min.), resulting in 13±5% RCY.

The $[Fe^{18}F^{19}F_2(BnMe_2\text{-tacn})]$ was purified using a solid phase extraction (SPE) protocol through an HLB cartridge to leave the ^{18}F-fluorinated metal-chelate as the single product. The stability of $[Fe^{18}F^{19}F_2(BnMe_2\text{-tacn})]$ was investigated in different formulation solutions (20:80 EtOH:water, 10:90 EtOH:PBS and 10:90 EtOH:HSA, Fig 8, Fig 9, Fig S53 and Fig S54), showing good stability over at least 2 hours with RCP = 99% for the EtOH/H_2O and EtOH/PBS, and RCP = 90% for EtOH/HSA. The target radioproduct could also be purified through a prep. HPLC system, giving the same RCP at t = 0 as in the SPE purification protocol.

Table 1 $^{18}F/^{19}F$ radiolabelling conditions. Reactions performed in 75:25 MeCN/target water. All experiments were performed at least 2 times.

$[FeF_3(BnMe_2\text{-tacn})]$ (mass/mg)	Scale (nmol)	T/°C (time/min)	RCY (%)
1	2360	25(10)	6±1
1	2360	80(10)	44±6
0.1	236	80(10)	40±6
0.01	24	80(10)	13±5

Conclusions

Evaluation of the stability of complexes of the type $[MF_3(L)]$, where M = Cr(III), Mn(III), Fe(III), Co(III) and L = terpy, Me_3-tacn, has been carried out by means of UV-vis spectroscopy. The compounds, including the new $[MnF_3(Me_3\text{-tacn})]$, $[FeF_3(terpy)]$, $[FeF_3(BnMe_2\text{-tacn})]$, $[CoF_3(L)]$ and $[CoCl_3(Me_3\text{-tacn})]$, have been synthesised and fully characterised. $[CoF_3(Me_3\text{-tacn})]$

represents the first structurally characterised Co(III) fluoride complex with a neutral N-donor ligand.

The possibility of obtaining the fluoride complexes from the chloride analogues by Cl/F exchange reactions on [MF_3(Me_3-tacn)] (M = Cr, Fe) was also explored. Although the bond dissociation energies of the M-F bonds are greater than the M-Cl bonds in all cases, the combination of thermodynamic and kinetic stability greatly affects the complexes and the outcome of the halide exchange reactions.

Stability tests performed on [MF_3(Me_3-tacn)] and [MF_3(terpy)] (M = Cr, Fe) have shown that the terpy complexes do not have the stability required to be a contender for future PET applications. This was also observed in the Group 13 (Al, Ga) and ScF_3 terpy complexes.[8,13] Among the complexes with Me_3-tacn as ligand, [FeF_3(Me_3-tacn)] and [CrF_3(Me_3-tacn)] showed good stability in most conditions; however, the reaction kinetics of the Cl/F exchange on [$CrCl_3$(Me_3-tacn)] using 4 mol. equiv. of [Me_4N]F in MeCN under reflux proved to be slow, with a mixture of the chloride and fluoride complexes present after 24 h. The d^5 system, [FeF_3(Me_3-tacn)], proved to be more successful. Fluorination was achieved within 30 mins. in aqueous MeCN at room temperature using KF as the fluoride source, causing complete conversion to [FeF_3(Me_3-tacn)].

Stability tests indicated that tacn derivatives bearing the FeF_3 fragment may be suitable for radiofluorination, and this was borne out by $^{18}F/^{19}F$ isotopic exchange reactions using [FeF_3($BnMe_2$-tacn)] at concentrations down to 24 nM. The resulting [$Fe^{18}F^{19}F_2$($BnMe_2$-tacn)] is stable in ethanolic PBS or HAS over at least 2 h. This constitutes the first example of a transition metal complex where radiofluorination is achieved through formation of a direct M-^{18}F bond.

Conflicts of interest

There are no conflicts to declare.

Acknowledgements

We thank the EPSRC and GE Healthcare for funding through a CASE studentship to F. M. M. (EP/L505651/1) and EPSRC for a doctoral prize (EP/R513325/1).

References

1 P. W. Miller, N. J. Long, R. Vilar and A. D. Gee, *Angew. Chem. Int. Ed.*, 2008, **47**, 8998.
2 J. D. G. Correia, A. Paulo, P. D. Raposinho and I. Santos, *Dalton Trans.*, 2011, **40**, 6144; R. Kumar, W. S. Shin, K. Sunwoo, W. Y. Kim, S. Koo, S. Bhuniya and J. S. Kim, *Chem. Soc. Rev.*, 2015, **44**, 6670.
3 G. E. Smith, H. L. Sladen, S. C. G. Biagini and P. J. Blower, *Dalton Trans.*, 2011, **40**, 6196; M. Glaser, P. Iveson, S. Hoppmann, B. Indrevoll, A. Wilson, J. Arukwe, A. Danikas, R. Bhalla and D. Hiscock, *J. Nucl. Med.*, 2013, **54**, 1981.
4 R. Ting, M. J. Adam, T. J. Ruth and D. M. Perrin, *J. Am. Chem. Soc.*, 2005, **127**, 13094; T. W. Hudnall, F. P. Gabbaï, *J. Am. Chem. Soc.*, 2007, **129**, 11978; A. Khoshnevisan, M. Jauregui-Osoro, K. Shaw, J. B. Torres, J. D. Young, N. K. Ramakrishnan, A. Jackson, G. E. Smith, A. Gee and P. J. Blower, *EJNMMI*, 2016, **6**, 34; J. O'Doherty, M. Jauregui-Osoro, T. Brothwood, T. Szyszko, P. K. Marsden, M. J. O'Doherty, G. J. R. Cook, P. J. Blower and V. Lewington, *J. Nucl. Med.*, 2017, **58**, 1666; Z. Li, K. Chansaenpak, S. Liu, C. R. Wade, P. S. Conti and F. P. Gabbaï, *Med. Chem. Commun.*, 2012, **3**, 1305; K. Chansaenpak, M. Wang, Z. Wu, R. Zaman, Z. Li and F. P. Gabbaï, *Chem. Commun.*, 2015, **51**, 12439; Z. Liu, M. Pourghiasian, M. A. Radtke, J. Lau, J. Pan, G. M. Dias, D. Yapp, K. S. Lin, F. Bénard and D. M. Perrin, *Angew. Chem. Int. Ed.*, 2014, **53**, 11876.
5 P. Leverman, W. McBride, R. Sharkey, A. Eek, L. Joosten, W. Oyen, D. Goldenberg, O. Boerman, *J. Nucl. Med.*, 2010, **50**, 454; W. McBride, C. D'Souza, R. Sharkey, H. Karacay, E. Rossi, C. Chang, D. Goldenberg, *Bioconjugate Chem.*, 2016, **21**, 1331; W. McBride, R. Sharkey, H. Karacay, C. D'Souza, E. Rossi, P. Laverman, C. Chang, O. Boerman, D. Goldenberg, *J. Nucl. Med.*, 2009, **50**, 991; W. McBride, C. D'Souza, H. Karacay, R. Sherkey, D. Goldenberg, *Bioconjugate Chem.*, 2012, **23**, 538.
6 W. Levason, S. K. Luthra, G. McRobbie, F. M. Monzittu and G. Reid, *Dalton Trans.*, 2017, **46**, 14519.
7 F. M. Monzittu, I. Khan, W. Levason, S. K. Luthra, G. McRobbie and G. Reid, *Angew. Chem. Int. Ed.*, 2018, **57**, 6658; R. Bhalla, W. Levason, S. K. Luthra, G. McRobbie, G. Sanderson and G. Reid, *Chem. Eur. J.*, 2015, **21**, 4688; R. Bhalla, C. Darby, W. Levason, S. K. Luthra, G. McRobbie, G. Reid and G. Sanderson, *Chem. Sci.*, 2014, **5**, 381.
8 T. K. Venkatachalam, P. V. Bernhardt, D. H. R. Stimson, G. K. Pierens, R. Bhalla and D. C. Reutens, *Aust. J. Chem.*, 2018, **71**, 81.
9 G. Pascali, L. Matesic, B. Zhang, A. T. King, A. J. Robinson, A. T. Ung and B. H. Fraser, *EJNMMI Radiopharmacy and Chemistry* 2017, **2**, 9; A. Khoshnevisan, K. Chuamsaamarkkee, M. Boudjemeline, A. Jackson, G. E. Smith, A. D. GE, G. D. Fruhwirth, P. J. Blower, *J. Nucl. Med.* 2017, **58**, 156.
10 R. Schirrmacher, G. Bradtmoller, E. Schirrmacher, O. Thews, J. Tillmanns, T. Siessmeier, H. G. Buchholz, P. Bartenstein, B. Wängler, C. M. Niemeyer and K. Jurkschat, *Angew. Chem. Int. Ed.*, 2006, **45**, 6047; C. Wängler, B. Waser, A. Alke, L. Iovkova, H. G. Buchholz, S. Niedermoser, K. Jurkschat, C. Fottner, P. Bertenstein, R. Schirrmacher, J. C. Reubi, H. J. Wester and B. Wängler, *Bioconjugate Chem.*, 2010, **21**, 2289; S. Niedermoser, J. Chin, C. Wängler, A. Kostikov, V. Bernard-Gauthier, N. Vogler, J. P. Soucy, A. J. McEwan, R. Schirrmacher and B. Wängler, *J. Nucl. Med.*, 2015, **56**, 1100.
11 K. Chansaenpak, B. Vabre and F. P. Gabbaï, *Chem. Soc. Rev.*, 2016, **45**, 954; V. Bernard-Gauthier, J. J. Bailey, Z. Liu, B. Wängler, C. Wängler, K. Jurkschat, D. M. Perrin and R. Schirrmacher, *Bioconjugate Chem.*, 2016, **27**, 267; V. Bernard-Gauthier, M. L. Lepage, B. Waengler, J. J. Bailey, S. H. Liang, D. M. Perrin, N. Vasdev and R. Schirrmacher, *J. Nucl. Med.*, 2018, **59**, 568.
12 R. Bhalla, W. Levason, S. K. Luthra, G. McRobbie, F. M. Monzittu, J. Palmer, G. Reid, G. Sanderson and W. Zhang, *Dalton Trans.*, 2015, **44**, 9569.
13 E. Curnock, W. Levason, M. E. Light, S. K. Luthra, G. McRobbie, F. M. Monzittu, G. Reid and R. N. Williams, *Dalton Trans.*, 2018, **47**, 6059.
14 P. Knopp and K. Wieghardt, *Z. Naturforsch.*, 1991, **46b**, 1077.
15 S. L. Benjamin, W. Levason and G. Reid, *Chem. Soc. Rev.*, 2013, **42**, 1460.
16 D. A. House and V. McKee, *Polyhedron*, 1993, **12**, 2335; J.V. Brencic, B. Ceh and I. Leban, *Monastsh. Chem.*, 1981, **12**, 1359; J. Glerup, J. Josephsen, K. Michelsen, E. Pedersen and C. E. Schaffer, *Acta Chem. Scand.*, 1970, **24**, 247; J. V. Brencic and I. Leban, *Z. Anorg. Allg. Chem.*, 1981, **480**, 213; J. W. Vaughn and J. Marzowski, *Inorg. Chem.*, 1973, **12**, 2346; J. W. Vaughn, *Inorg. Chem.*, 1981, **20**, 2397; H. L. Schlaefer, H. Gausmann

and H.U. Zander, *Inorg. Chem.*, 1967, **6**, 1528; C. E. Schaffer, J. M. Lang and H. G. Drickamer, *Inorg. Chem.*, 1996, **35**, 5072.
17 A. B. P. Lever, *Inorganic Electronic Spectroscopy*, Elsevier, 1984, Vol. 33.
18 H. X. Liu, *Acta Crystallogr., Sect. E: Struct. Rep. Online*, 2013, **65**, m1093.
19 K. S. Pedersen, G. Lorusso, J. J. Morales, T. Weyhermuller, S. Piligkos, S. K. Singh, D. Larsen, M. Schau-Magnussen, G. Rajaraman, M. Evangelisti and J. Bendix, *Angew. Chem. Int. Ed.*, 2014, **53**, 2394.
20 T. Birk, M. J. Magnussen, S. Piligkos, H. Weihe, A. Holten and J. Bendix, *J. Fluorine Chem.*, 2010, **131**, 898.
21 J. H. Choi and U. Lee, *Acta Crystallogr. Sect. E: Struct. Rep Online*, 2008, **64**, m1186; J. H. Choi, I. G. Oh, K. S. Ryoo, W. T. Lim, Y. C. Park and M. H. Habibi, *Spectrochim. Acta A*, 2006, **65**, 1138.
22 P. Nunez, C. Elias, J. Fuentes, X. Solans, A. Tressaud, M. C. M DeLucas and F. Rodriguez, *J. Chem. Soc., Dalton Trans.*, 1997, 4335.
23 A. R. Biju and M. V. Rajasekharan, *J. Mol. Struct.*, 2008, **875**, 456.
24 C. Mantel, S. K. Hassan, J. Pecaut, A. Deronzier, M. N. Collomb and C. Duboc-Toia, *J. Am. Chem. Soc.*, 2003, **125**, 12337.
25 K. S. Pedersen, M. Sigrist, H. Weihe, A. D. Bond, C. A. Thuesen, K. P. Simonsen, T. Birk, H. Mutka, A. L. Barra and J. Bendix, *Inorg. Chem.*, 2014, **53**, 5013.
26 K. S. Pedersen, M. A. Sorensen and J. Bendix, *Coord. Chem. Rev.*, 2015, **299**, 1.
27 F. Kraus and S. A. Baer, *Z. Naturforsch.*, 2011, **66b**, 865.
28 J. A. McCleverty and T. J. Meyer, *Comprehensive Coordination Chemistry II*, Pergamon, Oxford, 2004, Vol. 6.
29 Y. Mitsutsuka, E. Tursun and M. Nakahara, *Bull. Chem. Soc. Jpn.*, 1990, **63**, 260.
30 E. F. Murphy, R. Murugavel and H. W. Roesky, *Chem. Rev.*, 1997, **97**, 3425; N. M. Doherty and N. W. Hoffman, *Chem. Rev.*, 1991, **91**, 553; W. Massa and D. Babel, *Chem. Rev.*, 1988, **88**, 275; M. J. Molski and K. Seppelt, *Dalton Trans.*, 2009, 3379; M. Leblanc, V. Maisonneuve and A. Tressaud, *Chem. Rev.*, 2015, **115**, 1191.
31 B. N. Figgis and J. Lewis, *The Magnetic Properties of Transition Metal Complexes*, In *Prog. Inorg. Chem.*, John Wiley & Sons, Inc, 2007, pp 37-239.
32 J. Mason, *Multinuclear NMR*, ed. Plenum, New York, 1987.
33 N. Juranic, *J. Chem. Soc., Dalton Trans.*, 1984, 1537.
34 S. Bagger and H. P. Jensen, *Acta Chem. Scand.*, 1978, **32**, 659; T. Laier, C. E. Schaffer and J. Springborg, *Acta Chem. Scand.*, 1980, **34**, 343.